Research article

Explicating the recognition phenomenon of hazardous nitro-aromatic compound from contaminated environmental and cellular matrices by rationally designed pyridine-functionalized molecular probes

Amita Mondal [a,c,1,2], Abhijit Hazra [a,b,1], Mohit Kumar Chattopadhyay [a,1], Debojyoti Kundu [a,b], Swarup Kumar Tarai [c], Pritam Biswas [d], Ashish Bhattacharjee [d], Sukdeb Mandal [a,b], Priyabrata Banerjee [a,b,*,#]

[a] CSIR-Central Mechanical Engineering Research Institute, M. G. Avenue, Durgapur 713209, India
[b] Academy of Scientific and Innovative Research (AcSIR), AcSIR Headquarters CSIR-HRDC Campus, Postal Staff College Area, Sector 19, Kamla Nehru Nagar, Ghaziabad 201002, Uttar Pradesh, India
[c] Department of Chemistry, National Institute of Technology, M. G. Avenue, Durgapur 713209, India
[d] Department of Biotechnology, National Institute of Technology, M. G. Avenue, Durgapur 713209, India

ARTICLE INFO

ABSTRACT

In the quest of recognizing hazardous nitro-aromatic compounds in water, two pyridine-functionalized Schiff-base chemosensors, DMP ((E)-N-(3,4-dimethoxybenzylidene)(pyridin-2-yl) methanamine)) and MP (4-((E)-((pyridin-2-yl)methylimino)methyl)-2-ethoxyphenol) have been synthesized to detect mutagenic 2,4,6-Trinitrophenol (TNP) in soil, water as well as cellular matrices by producing turn-off emission responses as a combined consequence of PET and RET processes. Several experimental analyses including ESI-MS, FT-IR, photoluminescence, ^{1}H NMR titration, and the theoretical calculations ascertained the formation and sensing efficacies of the chemosensors. The analytical substantiations revealed that structural variation of the chemosensors played a significant role in improving the sensing efficiency, which would certainly be worthwhile in developing small molecular TNP sensors. The present work depicted that the electron density within the MP framework was more than that of DMP due to the intentional incorporation of –OEt and –OH groups. As a result, MP represented a strong interaction mode towards the electron-deficient TNP with a detection limit of 39 μM.

1. Introduction

The continual escalation of worldwide terrorist activities draws the attention of the scientific community toward the exploration of inexpensive, innovative, and competent chemosensors for on-field instantaneous recognition of explosives [1–4]. Nitro aromatic

explosives (NAEs) are the substances possessing nitro-functionalized benzene moiety, which are extensively used to prepare fireworks and matches, in forensic inquiries, and in the military and aviation industries, therefore can be easily accumulated in the natural water resources and other environmental matrices at the time of their usage, storage, testing, and dumping [5,6]. The growing intimidations regarding NAEs to the environment, including humans, and animals, have outstretched global concerns towards their prompt recognition, even in trace levels. Reportedly, the continued accumulation of NAEs may cause hemoglobin oxidation (methemoglobin) including anemia, and numerous adverse impacts on the liver and bladder [7,8]. 2,4,6-Trinitrophenol (TNP or picric acid), 2,4,6-tri-nitromethylbenzene (TNT), as well as 2,4-dinitrotoluene (DNT), are some common industrial NAEs which are ubiquitously present in explosive devices, including mine fillings, grenades, and bombs [2–5]. TNP, comprising strong electron-withdrawing groups, is the strongest organic acid and is found in fireworks, rocket fuel, the dye industry, chemical laboratories, pharmaceuticals, *etc*. [1,9]. After metabolization, TNP produces exceedingly harmful picramic acid byproduct, while its good water solubility (0.254 g/100 ml) made it a potent water and soil contaminant [10–12]. On account of its more explosive properties compared to TNT and analogous NAEs, the Environmental Protection Agency identified TNP as a potent cancer-causing agent and warned regarding its detrimental health impacts upon disproportionate ingestion [6,7,9,11,13]. Therefore, the acceptable concentration of TNP in potable water is 0.5 mg/L and the allowable daily intake (ADI) is 1–37 μg/kg, above which it may produce anemia, cancer, skin irritation, liver dysfunction, and respiratory organ impairment [9]. Nevertheless, despite its more fatal impacts than TNT, less consideration has been paid to recognizing TNP in comparison with TNT [8]. Moreover, selective, sensitive, and instant detection of TNP even in presence of TNT like other NAEs is relatively challenging due to their intrinsically comparable high electron affinity [5,8]. Therefore, the exploration of selective, fast-responsive, portable, and sensitive techniques for recognizing TNP is significantly important in the current scenario [8]. The hitherto explored versatile instrumental ultramicroscopic level TNP recognition practices; including Raman spectroscopy, X-ray scanning microscopy, atomic absorption and fluorescence spectrometry (AAS and AFS), inductively coupled surface enhanced resonance Raman spectroscopy (SERS), gas chromatography coupled with mass spectrometry (GC-MS), plasma mass spectrometry (ICPMS), ion mobility spectrometry (IMS), ion selective electrode (ISE), *etc*.; possess high cost, complicated sample preparation, lengthy response time, lack of transportability and larger sizes, limiting the on-spot analyte detection aptitude [14–17]. Therefore, reconnoitering multifunctional highly sensitive sensory probes for recognizing TNP is immensely urgent [16], while the fluorescence detection approach is specifically viable because of their several advantages, including, high sensitivity, real-time prompt responses, simplicity, and compactness [8,18–21].

Choosing an apposite chemosensor is essential to achieve the effectual recognition of the specific analyte [22]. Hence, numerous new fluorescent sensors have been explored for identifying TNP, for example, water-soluble Si nanoparticles, MoS_2 quantum dots, pyrenyl probes, Tb-functionalized carbon dots, MOFs, *etc*. Nonetheless, intricate operation, complex synthesis route, and high toxicity restricted their practical applications in the realm of aqueous phase TNP recognition [23]. Simultaneously, other fluorescent probes, like microporous metamemeworks (MOFs), dual-emission quantum dot hybrids, fluorescent film sensors, and conjugated polymers (CPs) are less viable owing to aggregation-caused quenching (ACQ), where the fluorescence intensity diminishes in presence of higher extent of luminophores [24,25]. As a consequence, the design and synthesis of luminescent small organic sensors can be a cutting-edge choice for developing more advantageous proficient chemosensors [25–28]. In this aspect, Schiff-base chemosensors, can be a potential contender for recognizing TNP due to their ease of synthesis, simplicity, high yield, stability, and tunability [29,30]. The Schiff-base sensors are well-explored for recognizing various target-specific analytes, however, recognizing TNP by Schiff-base sensory probes are still less explored in the literature [31,32].

In this background, two inventive pyridine-functionalized Schiff-base chemosensors DMP (E-N-(3,4-dimethoxybenzylidene)(pyridin-2-yl)methanamine) and MP (4-((E)-((pyridin-2-yl)methylimino)methyl)-2-ethoxyphenol) have been introduced herein with an eye of low-level recognition of TNP in the aqueous medium. Both the chemosensors represented high quenching efficiencies towards TNP in the pool of various other NAEs. Usually, the electron-deficient TNP molecule has the propensity to interact with the electron-rich molecule. Therefore, structural suitability is the fundamental approach to designing a superior chemosensor. In the case of MP, the predominating + R effect of –OH and lesser –I effect of the -OEt group enhanced the electron density within the framework. As a result, MP represented more recognition aptitude towards electron-deficient TNP by facilitating the electron transfer from the sensor toward the analyte framework. The formation of the chemosensors and the recognition events have been well substantiated by several sophisticated analytical tools and theoretical calculations. Moreover, both the chemosensors were also found to be effective for recognizing TNP in various water specimens as well as soil samples, emboldening their applications in the realm of on-field detection of TNP. Additionally, the non-toxic chemosensors were also found to be highly efficient for recognizing TNP in A549 Human Lungs Carcinoma Cells, enhancing their applications in the realm of biosensing [33,34]. Precisely, both the TNP selective chemosensors depicted enhanced improvements in compared to several recently explored sensory probes, in terms of aqueous phase detection at a very low concentration, and selectivity, as well as real-world applications including intracellular recognition.

2. Experimental

2.1. Materials

All the preparative chemicals, NAEs, and solvents have been procured from Alfa Aesar and Sigma Aldrich (Merck). The materials have been used as received.

2.2. Instrumentation

ESI-MS and FT-IR spectra were logged on Advion make compact mass spectrometer (serial no. 3013–0140) and PerkinElmer FT-IR Spectrum 100 spectrophotometer. UV–Vis and fluorescence spectroscopic studies were accomplished in Varian Cary-60 and PerkinElmer LS45 spectrophotometer respectively. The ^{1}H NMR spectra were recorded in Bruker-made NMR spectrometer. The *in vitro* studies were executed in a Zeiss observer Z1 microscope.

2.3. Preparation of DMP and MP

Both the Schiff base chemosensors (DMP and MP) were synthesized by the condensation reaction (Scheme 1) between the amine derivative (2-Picolylamine, 1 mmol) with another moiety of carbonyl compounds (3,4-Dimethoxybenzaldehyde, 1 mmol in cased of DMP and 3-Ethoxy-4-hydroxybenzaldehyde) in EtOH (40 ml) under reflux with stirring for 5–6 h. Yellow precipitate was formed which was obtained by filtration and washed with diethyl ether and then dried in a vacuum with 85% (for DMP) and 87% (for MP) yield. M. P.: 188 °C for DMP and 192 °C for MP. *m/z*: calcd: 256.12 (for DMP and MP) and obtained: 257.4 (for DMP+H$^+$) and 256.5 (for MP+H$^+$). ^{1}H NMR spectra in CD$_3$CN: [for DMP]: 3.65–3.94 (6H of OMe), 5.38 (1H of –CH), 7.75 (1H of = CH) and 6.59–8.57 (7Ar–H) and [for MP]: 3.77–3.79 (5H of OEt), 5.23 (1H of –CH), 7.68 (1H of = CH) and 6.72–8.52 (7Ar–H) and 8.29 (1H of OH) (Figs. S1–S3, ESI).

## 3. Results and discussion

3.1. Photostability

High photostability is a fundamental feature of the chemosensor to be considered for long-time exposures [35]. Therefore, the photostability of both DMP and MP have been investigated and the probes depicted notable fluorescence stability under UV lamp up to 1 h, alluring their effectual applications towards TNP detection even in the cellular matrices (Fig. S5, ESI).

3.2. Fluorimetric titration of DMP and MP with TNP

Under UV light both the unbound chemosensors (10^{-3} M) showed greenish illumination in ACN solvent, which were quenched upon the addition of 10^{-4} M aqueous TNP. All the other NAEs were apparently irresponsive, suggesting the selective sensing efficiencies of the sensors towards TNP (Fig. 1(a, b), S8, ESI). Accordingly, in the fluorescence titration experiments, the DMP and MP exhibited emission spectra at 450 and 460 nm respectively, which upon gradual addition of TNP diminished in intensity along with a remarkable red-shifting, suggesting enhanced ICT within the sensor-analyte adducts (Fig. 2(a, b)). The response of the sensors towards TNP has also been noted to be constant for a long-time period (Fig. S6, ESI). The fluorescence spectra clearly indicated that MP has more sensing efficiency towards TNP compared to DMP as a result of enhanced electron density within the framework, which has also been revealed from the detection limit and quenching constant values (Table 1, Fig. S8, ESI). The quantum yield of DMP and MP were also calculated to be 0.82 and 0.97 respectively (Fig. S7, Table S1, ESI).

3.3. FT-IR spectra analysis of DMP and MP in presence of TNP

In the FT-IR spectra, the occurrence of the peak at 1640 cm^{-1} (for DMP) and 1600 cm^{-1} (for MP) affirmed the presence of the –C=N- group within the chemosensors, while in the case of MP, the broad peak at 3200 cm^{-1} suggested the existence of –OH group
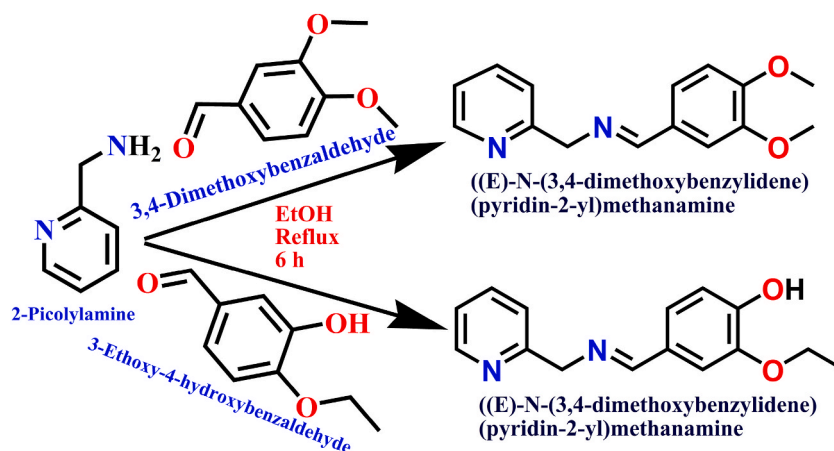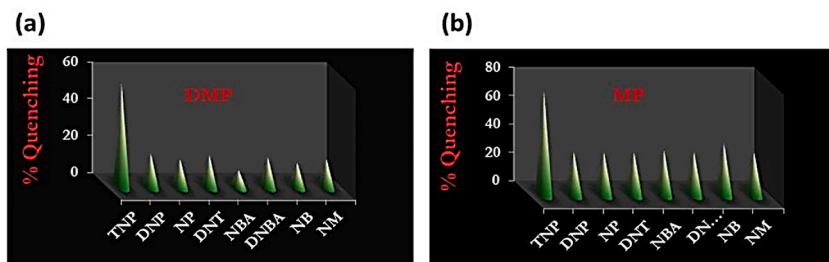

Scheme 1. Synthesis of DMP and MP.

Fig. 1. Selective fluorescence quenching of (a) DMP and (b) MP towards TNP in presence of other NAEs.
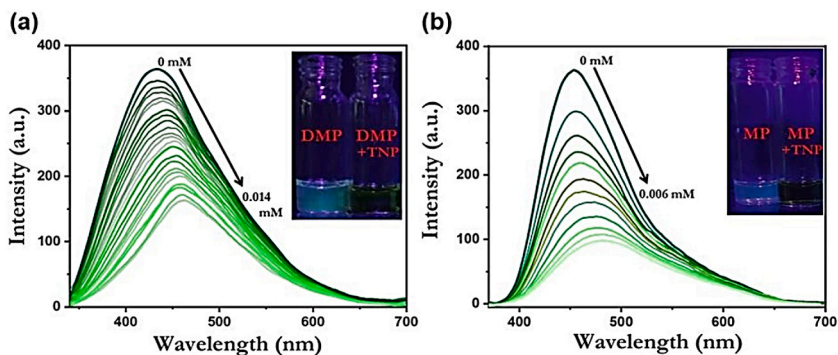

Fig. 2. Fluorescence quenching of (a) DMP and (b) MP in presence of TNP in ACN-H$_2$O media.

Table 1
Detection limit and quenching constant of DMP and MP.

Chemosensor	Limit of detection	Quenching constant
DMP	144 μM	1.18×10^5 M^{-1}
MP	39 μM	2.15×10^5 M^{-1}

[36]. After the addition of TNP, a new peak emerged at 3120 cm^{-1} corresponding to the phenolic –OH moiety, suggesting the formation of the sensor-analyte adducts (Fig. S4, ESI) [37]. However, all the other peaks at the aromatic region were intact validating no significant alteration of the sensory framework in presence of TNP.

3.4. ^{1}H NMR titration of DMP and MP in presence of TNP

In order to acquire a clear instigation regarding the mode of sensor-analyte interactions, ^{1}H NMR spectral titrations have been accomplished (Fig. 3(a, b)). In both cases, after the addition of TNP, the formation of a new peak at 8.7 ppm corresponding to the aromatic protons of TNP attributed the formation of host-guest adducts [38]. In the case of DMP, there was no significant spectral shifting in presence of TNP, suggesting a π–π stacking interaction between the sensor and TNP molecule. Likewise, TNP produced a
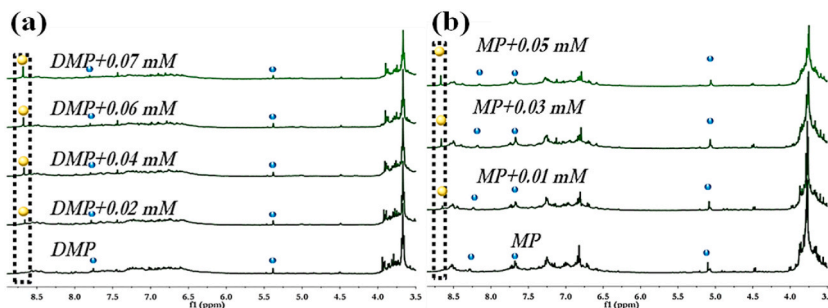

Fig. 3. ^{1}H NMR spectral titration of (a) DMP and (b) MP in presence of TNP in CD$_3$CN-D$_2$O medium.

stacking arrangement with MP also. Nonetheless, after the gradual addition of TNP with the MP solution, the peaks corresponding to –CH and =CH protons significantly shifted towards up field region along with all the aromatic and –OH protons accompanied by the downfield shifting of the aromatic protons of TNP, attributing to H-bonding interaction between the imine N of MP and the –OH proton of TNP [38–40]. As a result, MP represented better sensing efficiency towards TNP in comparison to DMP.

3.5. Theoretical corroboration

The theoretical calculations (carried out in Turbomole v7.0), carried out for determining the geometry-optimized structures of the sensors and sensor-analyte adducts, were completely in line with the experimental findings [41–43]. Upon the addition of TNP, the lowering of energy and the HOMO-LUMO gap of the sensors clearly attributed to the productive host-guest interaction (Table 2). The negative interaction energy (calculated by, $\Delta E = E_{A,B} - (E_A + E_B)$, where $E_{A,B}$ is the optimized energy of sensor-analyte assembly, E_A and E_B are the energies of sensor and analyte respectively) well-substantiated the feasible interaction processes. Interestingly, Lowdin population analysis clearly revealed that the imine N of MP was more electronegative compared to that of the DMP (Fig. S10, ESI) owing to the combined effects of OH and -OEt groups. In the case of DMP, the presence of the *m*-OMe group exerted a substantial –I effect while the +R effect of the *p*-OMe group facilitated the sensing process. Contrariwise, for MP, the existence of the *p*-OH group applied a superior +R effect, whereas the weaker electron withdrawing -OEt group played an additional advantage to enhance the electron density within the MP scaffold. As a result, in the case of DMP; electron-deficient TNP represented a stacking interaction at 6.963 Å, while it produced an H-bonding interaction with the imine N of MP at a bond length of 2.83 Å along with a stacking arrangement at a distance of 6.593 Å, suggesting more interaction efficiency between MP and TNP (Fig. 4(a–d), Scheme 2) [44–46]. The results have further been elucidated by RDG calculation (Fig. 5(a–d)) [47–49].

3.6. Mechanistic insights on recognizing TNP by DMP and MP

The quenching mechanisms of the chemosensors in presence of TNP can be attributed to synergistic electron transfer processes from the electro-rich sensor moieties towards the electron-deficient TNP molecule. Firstly, the photoinduced electron transfer (PET) has been affirmed from the DFT calculations, which clearly depicted that the LUMO energy level of the TNP molecule was much lower compared to that of the sensor molecules (Fig. 6, Scheme 2) [31]. Simultaneously, the non-linear S–V plot attributed the concomitant static and dynamic quenching process caused by the resonance energy transfer (RET), which has further been validated by the large overlap between the emission spectra of sensors and the absorbance spectra of TNP (Fig. 7(a–d)) [33].

3.7. Recognizing the presence of TNP in environmental specimens

A smart chemosensor must own numerous real-world applications. Detection of TNP in natural resources, like water, and soil samples is significant to develop a sustainable ecosystem. With the intention of exploring the practical applications of the chemosensors, various water, soil sample, and matches-powder have been collected and investigated [34]. The samples have been contaminated with 1 mM TNP and added to the chemosensor solutions. Remarkably, both DMP and MP exhibited significant quenching upon the addition of the TNP adulterated soil and water samples, encouraging their applications for on-field detection of TNP in various environmental matrices (Fig. 8(a, b)), Fig. S11).

3.8. Intracellular recognition of TNP by DMP and MP

TNP, the perilous environmental pollutant, can affect tissues and organs of the mammalian system. Wide utilization of TNP in several industries, including matches, leather, electric batteries, and dye industry can cause water and soil contamination [50,51]. Consequently, TNP can be accumulated in the human body via water and the food chain, which upon metabolization, produces more mutagenic picramic acid [52,53]. Therefore, in vitro detection of TNP is of significant necessity. In this context, DMP and MP, have been employed for recognizing TNP in A549 Human lungs carcinoma cells (Fig. 9(a–d)). Remarkably, the chemosensors incubated green emissive cells were observed to be quenched in presence of TNP, suggesting significant intracellular TNP recognition efficiencies of both DMP and MP.

Table 2
Geometry-optimized outcomes of DMP, MP and sensor-analyte adducts.

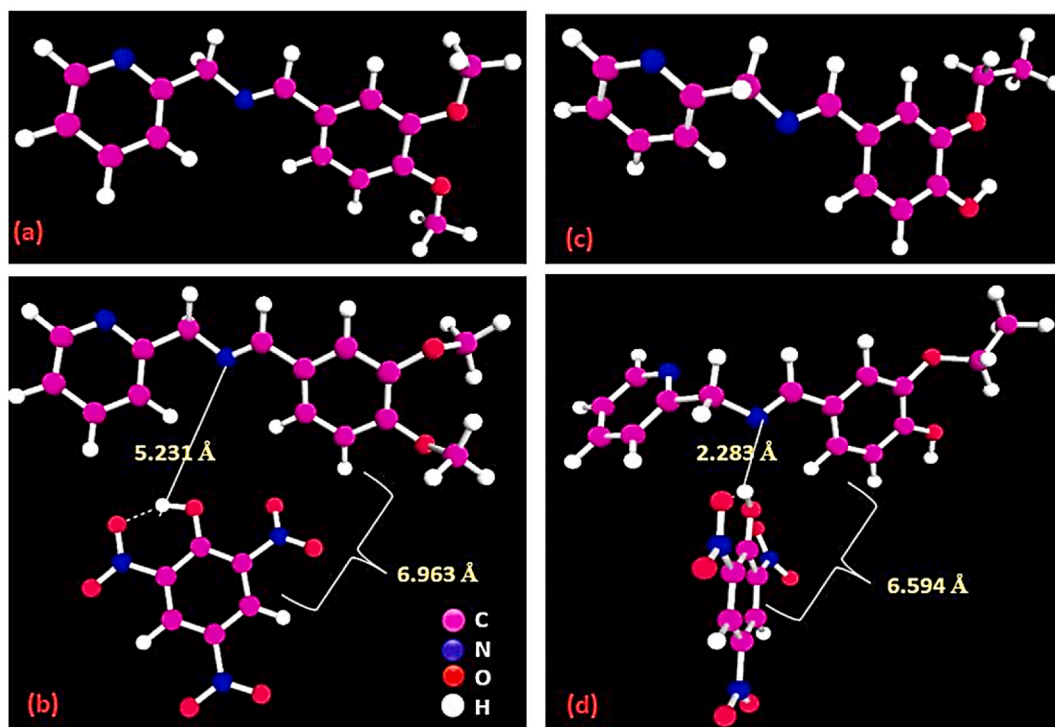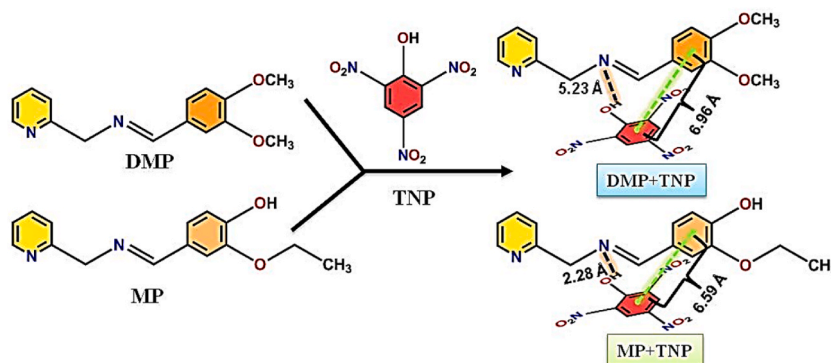|	Geometry-optimized energy (kJ/mol)	HOMO-LUMO gap (eV)	Interaction energy (kJ/mol)
TNP	−919.85	4.352	–
DMP	−840.01	4.484	−1.12
DMP + TNP	−1760.98	1.234	
MP	−840.03	4.561	−1.12
MP + TNP	−1761	1.197	

Fig. 4. Geometry optimized structures of (a) DMP, (b) DMP + TNP, (c) MP and (d) MP + TNP.

Scheme 2. Sensing Mechanism of DMP and MP with TNP.

3.9. Comparative literature analyses

Extensive literature studies have been performed to access the inimitability of this present work (vide Table 3). From Table 3, it is clearly observed that most of the explored sensory probes can detect TNP from the non-aqueous phase, while both DMP and MP were susceptible to detecting TNP in the aqueous phase with superior detection limit and prominent selectivity. A few of the explored sensors have been employed for real-field application, whereas both DMP and MP were perceived to have numerous practical applicability. In addition, intracellular detection of TNP by both sensors would unambiguously play a ground-breaking role in the domain of biomedical applications, which has not been well-explored previously. Apart from these, one of the major emphases of the present work was the structural modulation of the chemosensor by regulating electron density on the framework, which would provide a leading-edge footprint to design and develop a superior small molecular TNP selective chemosensor.

4. Conclusion

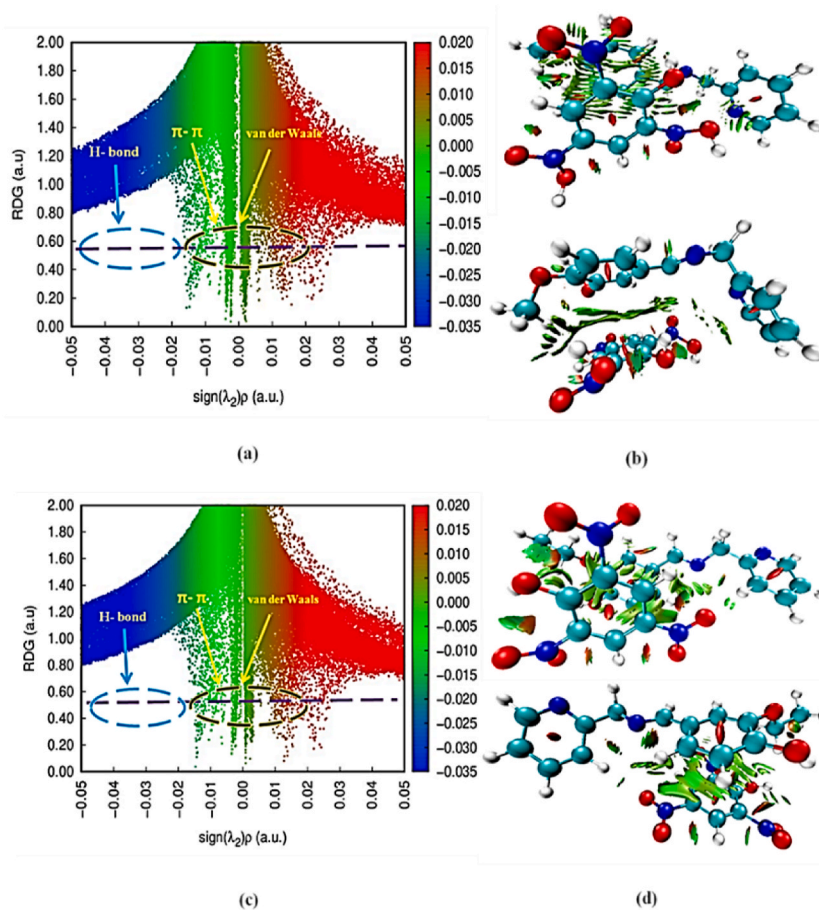Two inimitable Schiff-base chemosensors, DMP and MP have been introduced for recognizing aqueous phase TNP. Both the green

Fig. 5. RDG analysis for DMP-TNP and MP-TNP (a), (c) the scatter plot of RDG vs sign $(\lambda)\rho$ and color gradient and (b), (d) RDG gradient isosurface. (For interpretation of the references to color in this figure legend, the reader is referred to the Web version of this article.)
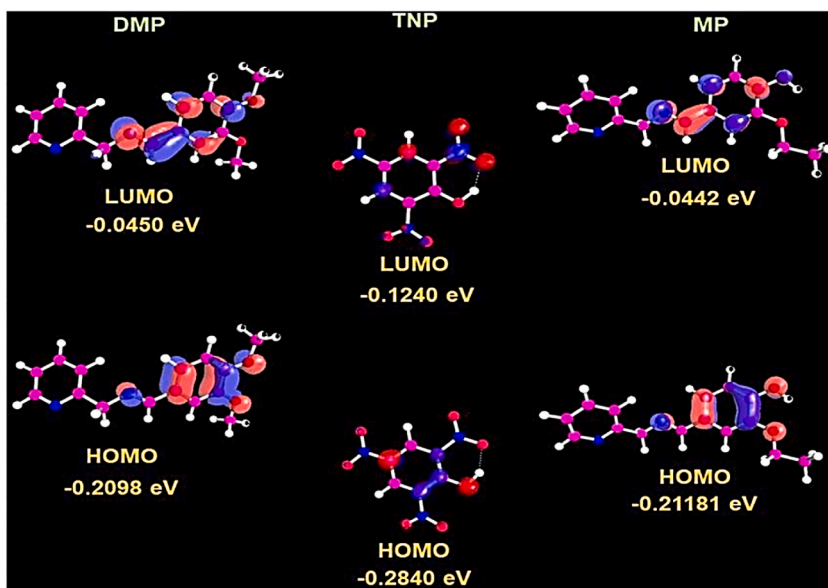

Fig. 6. Theoretical calculations affirming PET from the HOMO of the chemosenors towards TNP.
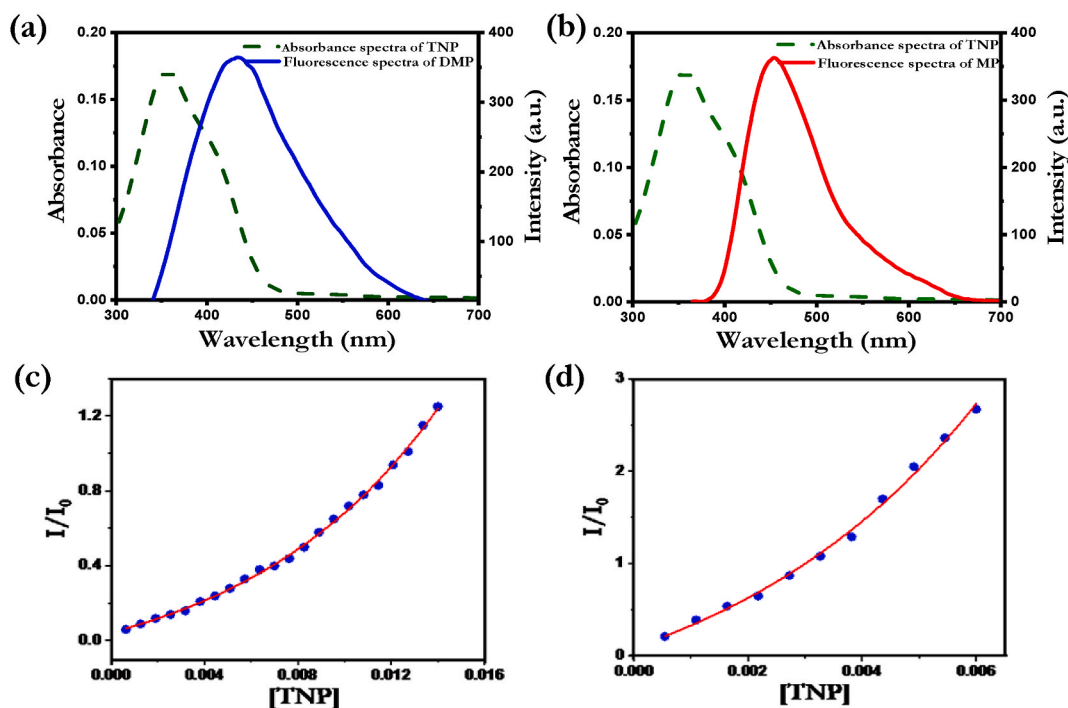
Fig. 7. Overlap between the emission spectra of (a) DMP and (b) MP and the absorbance spectra of TNP; Stern-Volmer (S–V) plots of (c) DMP and (d) MP in presence of TNP.
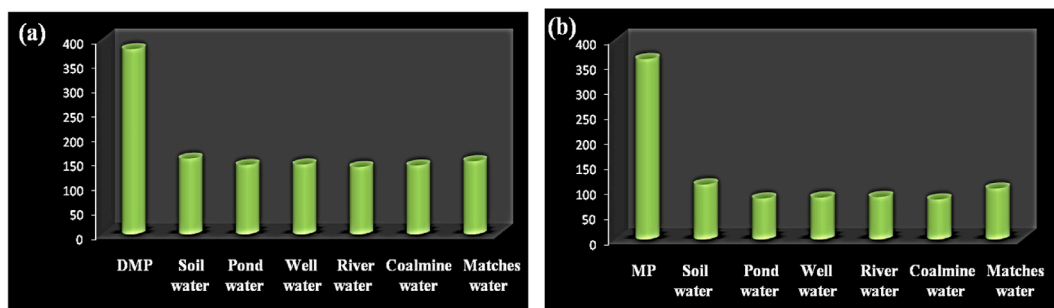

Fig. 8. Quenching of (a) DMP and (b) MP in presence of TNP contaminated environmental specimens

emissive chemosensors were observed to show significant quenching in presence of TNP, as a consequence of simultaneous PET and RET processes from the electron-rich sensor moieties towards the electron-deficient TNP molecule. Nonetheless, the MP framework was observed to have more electron density caused by the +R effect of the existing –OH group and the lesser –I effect generated by the –OEt group, producing comparatively stronger H-bonding interaction with TNP than DMP. Therefore, these structural modulations and consequent investigation would certainly be a noteworthy footprint for designing and developing proficient small molecular TNP sensors. All the experimental findings have further been validated by the DFT calculations. Additionally, both the sensors were capable to recognize TNP in contaminated soil and water samples, while intracellular recognition of TNP has also been carried out by using DMP and MP.

Author contribution statement

Amita Mondal, Abhijit Hazra, Mohit Kumar Chattopadhyay, Priyabrata Banerjee: Conceived and designed the experiments; Performed the experiments; Analyzed and interpreted the data; Contributed reagents, materials, analysis tools or data; Wrote the paper.

Debojyoti Kundu: Analyzed and interpreted the data; Contributed reagents, materials, analysis tools or data.

Swarup Kumar Tarai, Ashish Bhattacharjee: Analyzed and interpreted the data.

Pritam Biswas, Sukdeb Mandal: Contributed reagents, materials, analysis tools or data.
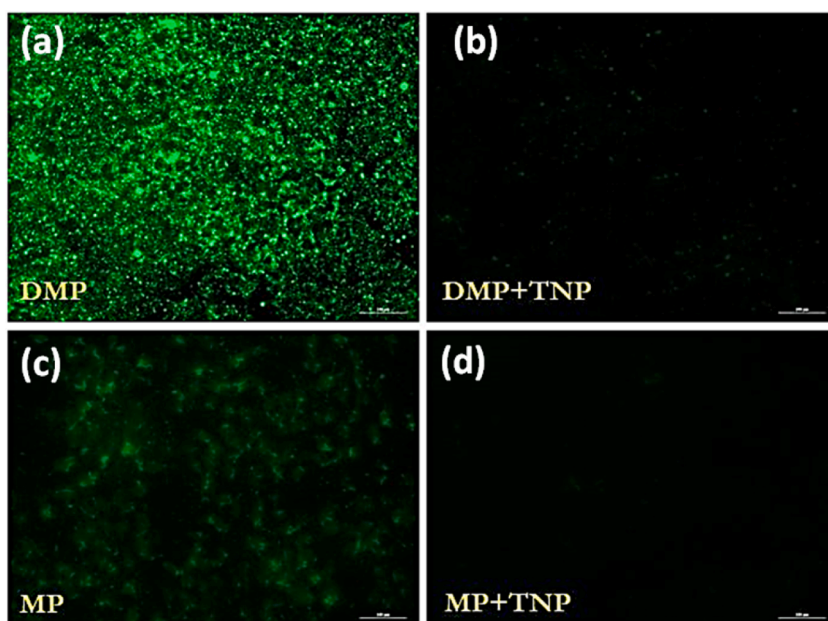
Fig. 9. Recognition of TNP by (a, b) DMP and (c, d) MP in A549 Human Lungs Carcinoma Cells.

Table 3
Comparative literature survey of hitherto explored TNP sensor.

SI. no.	Analytes detected	LOD	Detection medium	Real water analysis	*In vitro* detection by cell imaging	References
1.	TNP	0.017 μM	H_2O	Lake water	–	[54]
2.	TNP	0.12 μM	H_2O	–	–	[55]
3.	DNP, TNP	0.1613 μM	Acetonitrile	–	–	[26]
4.	Cu^{2+}, TNP	0.35 μM	Acetonitrile	–	In-vitro detection for Cu^{2+}	[38]
5.	TNP	0.57 μM	H_2O	–	–	[31]
6.	TNP	0.576 μM	Acetonitrile, Toluene	–	–	[28]
7.	Al^{3+}, Zn^{2+}, TNP	1.74 μM	H_2O- THF	–	–	[56]
8.	TNP	70 μM	DMSO	–	–	[57]
9.	TNP	99 μM	H_2O	–	–	[27]
10.	TNP	370 μM	H_2O	–	–	[58]
11.	TNP, Cu^{2+}	2410 μM	DMF	–	–	[59]
12.	TNP	144 μM, 39 μM	H_2O	Soil sample, Pond water, Coal mine water, Well water, River water	In-vitro detection	This Work

Data availability statement

The data that has been used is confidential.

Declaration of interest's statement

The authors declare that they have no known competing financial interests or personal relationships that could have appeared to influence the work reported in this paper.

Acknowledgment

Appendix A. Supplementary data

Supplementary data to this article can be found online at https://doi.org/10.1016/j.heliyon.2023.e13620.

References

[1] M.-Y. Zhang, R.-D. Dai, B.-J. Li, T.-X. Hang, J.-X. Xie, J. Lü, X.-D. Zhu, Fluorescent metal–organic framework constructed from semi-rigid ligand for the sensitive sensing of 2,4,6-trinitrophenol, Cryst. Growth Des. 20 (2020) 1373–1377, https://doi.org/10.1021/acs.cgd.9b01379.

[2] P. Das, S.K. Mandal, Strategic design and functionalization of an amine-decorated luminescent metal organic framework for selective gas/vapor sorption and nanomolar sensing of 2,4,6-trinitrophenol in water, ACS Appl. Mater. Interfaces 10 (2018) 25360–25371, https://doi.org/10.1021/acsami.8b06339.

[3] L. Martelo, T. das Neves, J. Figueiredo, L. Marques, A. Fedorov, A. Charas, M. Berberan-Santos, H. Burrows, Towards the development of a low-cost device for the detection of explosives vapors by fluorescence quenching of conjugated polymers in solid matrices, Sensors 17 (2017) 2532, https://doi.org/10.3390/s17112532.

[4] L.M. Martelo, L.F. Marques, H.D. Burrows, M.N. Berberan-Santos, Explosives detection: from sensing to response, in: B. Pedras (Ed.), Fluoresc. Ind., Springer International Publishing, Cham, 2019, pp. 293–320, https://doi.org/10.1007/4243_2019_9.

[5] J.-W. Liu, Y.-M. Wang, L. Xu, L.-Y. Duan, H. Tang, R.-Q. Yu, J.-H. Jiang, Melanin-like nanoquencher on graphitic carbon nitride nanosheets for tyrosinase activity and inhibitor assay, Anal. Chem. 88 (2016) 8355–8358, https://doi.org/10.1021/acs.analchem.6b01667.

[6] D. Peng, L. Zhang, F.-F. Li, W.-R. Cui, R.-P. Liang, J.-D. Qiu, Facile and green approach to the synthesis of boron nitride quantum dots for 2,4,6-trinitrophenol sensing, ACS Appl. Mater. Interfaces 10 (2018) 7315–7323, https://doi.org/10.1021/acsami.7b15250.

[7] R. Batool, N. Riaz, H.M. Junaid, M.T. Waseem, Z.A. Khan, S. Nawazish, U. Farooq, C. Yu, S.A. Shahzad, Fluorene-Based fluorometric and colorimetric conjugated polymers for sensitive detection of 2,4,6-trinitrophenol explosive in aqueous medium, ACS Omega 7 (2022) 1057–1070, https://doi.org/10.1021/acsomega.1c05644.

[8] X. Cao, N. Zhao, H. Lv, Q. Ding, A. Gao, Q. Jing, T. Yi, Strong blue emissive supramolecular self-assembly system based on naphthalimide derivatives and its ability of detection and removal of 2,4,6-trinitrophenol, Langmuir 33 (2017) 7788–7798, https://doi.org/10.1021/acs.langmuir.7b01927.

[9] Y. Han, Y. Chen, J. Feng, J. Liu, S. Ma, X. Chen, One-pot synthesis of fluorescent silicon nanoparticles for sensitive and selective determination of 2,4,6-trinitrophenol in aqueous solution, Anal. Chem. 89 (2017) 3001–3008, https://doi.org/10.1021/acs.analchem.6b04509.

[10] S. Senthilkumar, R. Goswami, V.J. Smith, H.C. Bajaj, S. Neogi, Pore wall-functionalized luminescent Cd(II) framework for selective CO_2 adsorption, highly specific 2,4,6-trinitrophenol detection, and colorimetric sensing of Cu^{2+} ions, ACS Sustain. Chem. Eng. 6 (2018) 10295–10306, https://doi.org/10.1021/acssuschemeng.8b01646.

[11] A.H. Malik, S. Hussain, A. Kalita, P.K. Iyer, Conjugated polymer nanoparticles for the amplified detection of nitro-explosive picric acid on multiple platforms, ACS Appl. Mater. Interfaces 7 (2015) 26968–26976, https://doi.org/10.1021/acsami.5b08068.

[12] S. Dhiman, M. Ahmad, G. Kumar, V. Luxami, P. Singh, S. Kumar, Ratiometric chemosensor for differentiation of TNP from other NACs using distinct blue fluorescence and visualization of latent fingerprints, J. Mater. Chem. C 9 (2021) 1097–1106, https://doi.org/10.1039/D0TC04795C.

[13] J. Zhang, Y. Liu, J. Feng, L. Gong, M.G. Humphrey, C. Zhang, Decanuclear cluster-based metal–organic framework with a (3,11)-connected topology and highly sensitive 2,4,6-trinitrophenol detection, Inorg. Chem. 58 (2019) 9749–9755, https://doi.org/10.1021/acs.inorgchem.9b00745.

[14] P.A. Abramov, A.S. Novikov, M.N. Sokolov, Interactions of aromatic rings in the crystal structures of hybrid polyoxometalates and Ru clusters, CrystEngComm 23 (2021) 6409–6417, https://doi.org/10.1039/D1CE00716E.

[15] A. Dutta, A. Singh, X. Wang, A. Kumar, J. Liu, Luminescent sensing of nitroaromatics by crystalline porous materials, CrystEngComm 22 (2020) 7736–7781, https://doi.org/10.1039/D0CE01087A.

[16] G. Zhang, L. Gao, H. Chai, Y. Ren, Novel multifunctional samarium–organic framework for fluorescence sensing of Ag^+, MnO_4^-, and cimetidine and electrochemical sensing of *o* -nitrophenol in aqueous solutions, ACS Omega 6 (2021) 6810–6816, https://doi.org/10.1021/acsomega.0c05867.

[17] P. Das, S.K. Mandal, Understanding the effect of an amino group on the selective and ultrafast detection of TNP in water using fluorescent organic probes, J. Mater. Chem. C 6 (2018) 3288–3297, https://doi.org/10.1039/C7TC05852G.

[18] J.-M. Liu, J.-X. Hou, J. Liu, X. Jing, L.-J. Li, J.-L. Du, Pyrazinyl-functionalized Zr(iv)-MOF for ultrasensitive detection of tyrosine/TNP and efficient CO_2/N_2 separation, J. Mater. Chem. C 7 (2019) 11851–11857, https://doi.org/10.1039/C9TC03096D.

[19] S. Sekar, P. Gawas, S.V. Bhat, V. Nutalapati, Highly fluorescent 2D-BCNO sheets based chemical sensor for selective detection of the explosive Dunnite and 4-nitrophenol in aqueous medium, Environ. Sci. Nano 8 (2021) 2908–2919, https://doi.org/10.1039/D1EN00391G.

[20] R. Golbedaghi, G.O. Ildiz, R. Azadbakht, R. Fausto, A new tetramine bis(2-naphthol)-derivative fluorescent chemosensor for aluminum ion (Al^{3+}), J. Mol. Struct. 1250 (2022), 131775, https://doi.org/10.1016/j.molstruc.2021.131775.

[21] S. Dey, A. Kumar, P.K. Mondal, K.M. Modi, D. Chopra, V.K. Jain, An oxacalix[4]arene derived dual sensing fluorescent probe for the detection of As(v) and Cr (vi) oxyanions in aqueous media, Dalton Trans. 49 (2020) 7459–7466, https://doi.org/10.1039/D0DT00452A.

[22] X. Wang, M. Lei, T. Zhang, Q. Zhang, R. Zhang, M. Yang, A water-stable multi-responsive luminescent Zn-MOF sensor for detecting TNP, NZF and $Cr_2O_7^{2-}$ in aqueous media, Dalton Trans. 50 (2021) 3816–3824, https://doi.org/10.1039/D0DT03049J.

[23] B. Qu, Z. Mu, Y. Liu, Y. Liu, R. Yan, J. Sun, Z. Zhang, P. Li, L. Jing, The synthesis of porous ultrathin graphitic carbon nitride for the ultrasensitive fluorescence detection of 2,4,6-trinitrophenol in environmental water, Environ. Sci. Nano 7 (2020) 262–271, https://doi.org/10.1039/C9EN01165J.

[24] W. Che, G. Li, X. Liu, K. Shao, D. Zhu, Z. Su, M.R. Bryce, Selective sensing of 2,4,6-trinitrophenol (TNP) in aqueous media with "aggregation-induced emission enhancement" (AIEE)-active iridium(iii) complexes, Chem. Commun. 54 (2018) 1730–1733, https://doi.org/10.1039/C7CC08832A.

[25] L.-L. Wen, X.-G. Hou, G.-G. Shan, W.-L. Song, S.-R. Zhang, H.-Z. Sun, Z.-M. Su, Rational molecular design of aggregation-induced emission cationic Ir(iii) phosphors achieving supersensitive and selective detection of nitroaromatic explosives, J. Mater. Chem. C 5 (2017) 10847–10854, https://doi.org/10.1039/C7TC03535G.

[26] P.D. Jawale Patil, R.D. Ingle, S.M. Wagalgave, R.S. Bhosale, S.V. Bhosale, R.P. Pawar, S.V. Bhosale, A naphthalimide-benzothiazole conjugate as colorimetric and fluorescent sensor for selective trinitrophenol detection, Chemosensors 7 (2019) 38, https://doi.org/10.3390/chemosensors7030038.

[27] A. Kathiravan, A. Gowri, T. Khamrang, M.D. Kumar, N. Dhenadhayalan, K.-C. Lin, M. Velusamy, M. Jaccob, Pyrene-Based chemosensor for picric acid—fundamentals to smartphone device design, Anal. Chem. 91 (2019) 13244–13250, https://doi.org/10.1021/acs.analchem.9b03695.

[28] R. Sodkhomkhum, M. Masik, S. Watchasit, C. Suksai, J. Boonmak, S. Youngme, N. Wanichacheva, V. Ervithayasuporn, Imidazolylmethylpyrene sensor for dual optical detection of explosive chemical: 2,4,6-Trinitrophenol, Sens. Actuators B: Chem. 245 (2017) 665–673, https://doi.org/10.1016/j.snb.2017.01.120.

[29] R. Golbedaghi, L.L.G. Justino, M. Bahrampour, R. Fausto, A novel fluorescent chemosensor for Cu^{2+} ion based on a new hexadentate ligand receptor: X-ray single crystal of the perchlorate salt of the ligand, ion selectivity assays and TD-DFT study, Inorg. Chim. Acta 515 (2021) 120061, https://doi.org/10.1016/j.ica.2020.120061.

[30] A. Bil, J. Gregoliński, M. Biczysko, Internal hydrogen bond influences the formation of [2+2] Schiff base macrocycle: open-chain vs. Hemiaminal and macrocycle forms: internal hydrogen bond influences the formation of [2+2] Schiff base macrocycle: open-chain vs. Hemiaminal and macrocycle forms, Eur. J. Org. Chem. 2019 (2019) 2243–2252, https://doi.org/10.1002/ejoc.201801811.

[31] Z.-H. Fu, Y.-W. Wang, Y. Peng, Two fluorescein-based chemosensors for the fast detection of 2,4,6-trinitrophenol (TNP) in water, Chem. Commun. 53 (2017) 10524–10527, https://doi.org/10.1039/C7CC05966C.

[32] S. Halder, P. Ghosh, A. Hazra, P. Banerjee, P. Roy, A quinoline-based compound for explosive 2,4,6-trinitrophenol sensing: experimental and DFT-D3 studies, New J. Chem. 42 (2018) 8408–8414, https://doi.org/10.1039/C8NJ00817E.

[33] M.M. Calabretta, D. Gregucci, H. Martínez-Pérez-Cejuela, E. Michelini, A luciferase mutant with improved brightness and stability for whole-cell bioluminescent biosensors and in vitro biosensing, Biosensors 12 (2022) 742, https://doi.org/10.3390/bios12090742.

[34] S. Dhibar, P. Yadav, T. Paul, K. Sarkar, A.P. Chattopadhyay, A. Krawczuk, B. Dey, A bio-relevant supramolecular Co(ii)-complex for selective fluorescence sensing of μM range inorganic As(iii) in aqueous medium and its intracellular tracking in bacterial systems, Dalton Trans. 48 (2019) 4362–4369, https://doi.org/10.1039/C8DT04127J.

[35] A.K. Mahapatra, P. Karmakar, J. Roy, S. Manna, K. Maiti, P. Sahoo, D. Mandal, Colorimetric and ratiometric fluorescent chemosensor for fluoride ions based on phenanthroimidazole (PI): spectroscopic, NMR and density functional studies, RSC Adv. 5 (2015) 37935–37942, https://doi.org/10.1039/C5RA05327G.

[36] A. Mondal, A. Hazra, J. Chakrabarty, N.C. Murmu, P. Banerjee, A harmonized applied and theoretical exploration for nanomolar level recognition of perilous F^- and CN^- by multichannel chemosensor: proposition of Hg^{2+}-mediated logic gate imitator, ChemistrySelect 5 (2020) 11976–11985, https://doi.org/10.1002/slct.202002964.

[37] A.K. Parmar, N.N. Valand, K.B. Solanki, S.K. Menon, Picric acid capped silver nanoparticles as a probe for colorimetric sensing of creatinine in human blood and cerebrospinal fluid samples, Analyst 141 (2016) 1488–1498, https://doi.org/10.1039/C5AN02303C.

[38] B.K. Kundu, P. Pragti, R. Reena, S.M. Mobin, S. Mukhopadhyay, Mechanistic and thermodynamic aspects of a pyrene-based fluorescent probe to detect picric acid, New J. Chem. 43 (2019) 11483–11492, https://doi.org/10.1039/C9NJ02342A.

[39] T.K. Ghosh, S. Jana, A. Ghosh, Exploitation of the flexidentate nature of a ligand to synthesize Zn(II) complexes of diverse nuclearity and their use in solid-state naked eye detection and aqueous phase sensing of 2,4,6-trinitrophenol, Inorg. Chem. 57 (2018) 15216–15228, https://doi.org/10.1021/acs.inorgchem.8b02497.

[40] N. Jiang, G. Li, W. Che, D. Zhu, Z. Su, M.R. Bryce, Polyurethane derivatives for highly sensitive and selective fluorescence detection of 2,4,6-trinitrophenol (TNP), J. Mater. Chem. C 6 (2018) 11287–11291, https://doi.org/10.1039/C8TC04250K.

[41] A.K. Sakr, H.V. Snelling, N.A. Young, Experimental evidence for the molecular molybdenum fluorides MoF to MoF_6: a matrix isolation and DFT investigation, New J. Chem. 46 (2022) 9666–9684, https://doi.org/10.1039/D1NJ06062G.

[42] B. Fetouhi, B. Haddad, S.A. Brandán, A. Paolone, D. Villemin, M. Boumediene, M. Rahmouni, S. Bresson, Synthesis, molecular structure, and properties of DABCO bromide based ionic liquid combining spectroscopic studies with DFT calculations, J. Mol. Struct. 1233 (2021), 130102, https://doi.org/10.1016/j.molstruc.2021.130102.

[43] K. Kacim, C. Jelsch, C. Lucas, F. Lefebvre, W. Kaminsky, C. Ben Nasr, K. Kaabi, Synthesis, crystal structure determination, DFT calculation, and Hirshfeld surface analysis of a new Zn(II) complex with the guaninium ligand, J. Coord. Chem. 73 (2020) 3307–3321, https://doi.org/10.1080/00958972.2020.1844192.

[44] D. Piovesan, G. Minervini, S.C.E. Tosatto, The RING 2.0 web server for high quality residue interaction networks, Nucleic Acids Res. 44 (2016) W367–W374, https://doi.org/10.1093/nar/gkw315.

[45] Y. Zhao, J. Li, H. Gu, D. Wei, Y. Xu, W. Fu, Z. Yu, Conformational preferences of π–π stacking between ligand and protein, analysis derived from crystal structure data geometric preference of π–π interaction, Interdiscip. Sci. Comput. Life Sci. 7 (2015) 211–220, https://doi.org/10.1007/s12539-015-0263-z.

[46] G.B. McGaughey, M. Gagné, A.K. Rappé, pi-Stacking interactions. Alive and well in proteins, J. Biol. Chem. 273 (1998) 15458–15463, https://doi.org/10.1074/jbc.273.25.15458.

[47] M. Lu, P. Zhou, Z. Li, J. Liu, Y. Yang, K. Han, New insights into the sensing mechanism of a phosphonate pyrene chemosensor for TNT, Phys. Chem. Chem. Phys. 20 (2018) 19539–19545, https://doi.org/10.1039/C8CP01749B.

[48] M. Lu, P. Zhou, Y. Ma, Z. Tang, Y. Yang, K. Han, Reconsideration of the detection and fluorescence mechanism of a pyrene-based chemosensor for TNT, J. Phys. Chem. 122 (2018) 1400–1405, https://doi.org/10.1021/acs.jpca.7b11739.

[49] M. Lu, X. Zhang, P. Zhou, Z. Tang, Y. Qiao, Y. Yang, J. Liu, Theoretical insights into the sensing mechanism of a series of terpyridine-based chemosensors for TNP, Chem. Phys. Lett. 725 (2019) 45–51, https://doi.org/10.1016/j.cplett.2019.03.041.

[50] R. Guo, L. Gao, J. Liang, Z. Zhang, J. Zhang, X. Niu, T. Hu, Two tetranuclear Cd-based metal–organic frameworks for sensitive sensing of TNP/Fe^{3+} in aqueous media and gas adsorption, CrystEngComm 22 (2020) 6927–6934, https://doi.org/10.1039/D0CE01193B.

[51] A. Hazra, S. Bej, A. Mondal, N.C. Murmu, P. Banerjee, Discerning detection of mutagenic biopollutant TNP from water and soil samples with transition metal-containing luminescence metal–organic frameworks, ACS Omega 5 (2020) 15949–15961, https://doi.org/10.1021/acsomega.0c01194.

[52] I. Kaur, V. Sharma, S.M. Mobin, P. Kaur, K. Singh, Excitation wavelength based reversible multicolour photoluminescence by a single chromophore upon aggregation: detection of picric acid-application in bioimaging, Sens. Actuators B: Chem. 281 (2019) 613–622, https://doi.org/10.1016/j.snb.2018.10.161.

[53] K. Maiti, A.K. Mahapatra, A. Gangopadhyay, R. Maji, S. Mondal, S.S. Ali, S. Das, R. Sarkar, P. Datta, D. Mandal, Simple bisthiocarbonohydrazone as a sensitive, selective, colorimetric, and ratiometric fluorescent chemosensor for picric acids, ACS Omega 2 (2017) 1583–1593, https://doi.org/10.1021/acsomega.6b00288.

[54] Y. Xiao, X. Yang, X. Cheng, S. Xiong, R. Chen, Fluorescent macromolecular chemosensors for highly and selectively detecting of 2, 4, 6-trinitrophenol, Mater. Res. Express 7 (2020), 105304, https://doi.org/10.1088/2053-1591/abbbab.

[55] H. Liu, Y. Fu, W. Xu, Q. He, H. Cao, G. Liu, J. Cheng, Microcrystal induced emission enhancement of a small molecule probe and its use for highly efficient detection of 2,4,6-trinitrophenol in water, Sci. China Chem. 61 (2018) 857–862, https://doi.org/10.1007/s11426-017-9223-2.

[56] S. Dey, A. Maity, M. Shyamal, D. Das, S. Maity, P.K. Giri, N. Mudi, S.S. Samanta, P. Hazra, A. Misra, An antipyrine based fluorescence "turn-on" dual sensor for Zn^{2+} and Al^{3+} and its selective fluorescence "turn-off" sensing towards 2,4,6-trinitrophenol (TNP) in the aggregated state, Photochem. Photobiol. Sci. 18 (2019) 2717–2729, https://doi.org/10.1039/c9pp00226j.

[57] S. Nath, S.K. Pathak, B. Pradhan, R.K. Gupta, K.A. Reddy, G. Krishnamoorthy, A.S. Achalkumar, A sensitive and selective sensor for picric acid detection with a fluorescence switching response, New J. Chem. 42 (2018) 5382–5394, https://doi.org/10.1039/C7NJ05136K.

[58] Z. Luo, B. Liu, S. Si, Y. Lin, C.S. Luo, C. Pan, C. Zhao, L. Wang, A fluorescent chemosensor based on nonplanar donor-acceptor structure for highly sensitive and selective detection of picric acid in water, Dyes Pigments 143 (2017) 463–469, https://doi.org/10.1016/j.dyepig.2017.05.002.

[59] J. Zhang, J. Wu, G. Tang, J. Feng, F. Luo, B. Xu, C. Zhang, Multiresponsive water-stable luminescent Cd coordination polymer for detection of TNP and Cu^{2+}, Sens. Actuators: B Chem. 272 (2018) 166–174, https://doi.org/10.1016/j.snb.2018.05.121.